



The impact of implantation depth of the Lotus™ valve on mechanical stress in close proximity to the bundle of His

Orla M. McGee¹ · Paul S. Gunning^{1,2} · Adrian McNamara² · Laoise M. McNamara¹

Received: 12 April 2018 / Accepted: 1 August 2018 / Published online: 20 August 2018
© Springer-Verlag GmbH Germany, part of Springer Nature 2018

Abstract

It has been proposed that inappropriate positioning of transcatheter aortic valves (TAVs) is associated with procedural complications and decreased device durability. Second-generation TAVs allow for repositioning giving greater control over the final deployment position. However, the impact of positioning on the tissue surrounding these devices needs to be better understood, in particular for the interleaflet triangle in which the conductance system (bundle of His) resides. In this study, we investigate the impact of implantation depth on the frame–tissue interaction for a next-generation repositionable Lotus™ valve. For this purpose, a computational model simulating deployment of the Lotus valve frame into a calcified patient-specific aortic root geometry was generated to predict aortic root stress and frame eccentricity at three different deployment depths. The results of this study predicted that positioning of the Lotus valve had an influence on the stresses in the aortic sinus and frame eccentricity. An analysis of levels of stress arising in the vicinity of the bundle of His, as a function of implantation depth, was conducted, and it was found that, for the specific patient anatomy studied, although the sub-annular position showed reduced peak stress in the aortic sinus, this implantation position showed the highest stress in the area of greatest risks of conductance interference. In contrast, while a supra-annular position increased the peak arterial stress, this implantation position resulted in lower stress in the interleaflet triangle and thus might reduce the risk of conductance interference. These results provide pre-operative information that can inform clinical decision-making regarding TAVI positioning.

Keywords Transcatheter aortic valve replacement · Transcatheter aortic valve implantation · Patient-specific · Finite element modelling · Lotus valve

1 Introduction

Aortic stenosis is a degenerative disease of the aortic heart valve associated with the build-up of calcium deposits on the leaflets of the aortic valve. Aortic stenosis is most often treated using a surgical aortic valve replacement (SAVR), a procedure requiring invasive open heart surgery (Walther et al. 2012). However, approximately 30% of patients are refused this surgery due to the fact that it is highly invasive and poses significant risk to elderly patients (Iung et al. 2003). Transcatheter aortic heart valve implantation (TAVI)

is a minimally invasive alternative to SAVR in the treatment of aortic stenosis.

The aortic valve is located between the mitral valve and the ventricular septum (Piazza et al. 2008). The close proximity and the potential for interference with the structures of the native valve anatomy make positioning of TAVs crucial for valve performance and patient outcomes. Indeed, recent studies have shown that incorrect positioning of TAVs can cause adverse effects such as the migration of the heart valve into the left ventricle, mitral insufficiency due to the expansion of the aortic valve under TAV implantation, arrhythmias, paravalvular leakage, prosthesis embolisation or aortic injury (Block 2010; Cao et al. 2012; Généreux et al. 2013; Masson et al. 2009). An increase in occurrence of conductance pathway disorders (left bundle branch block, LBBB) has also been observed when TAVI-treated patients were compared to those with surgical valve replacements. Incidences of new-onset LBBB have been reported to be between 8 and 30% for balloon-expandable valves (438 patients from 5 stud-

✉ Laoise M. McNamara
laoise.mcnamara@nuiagalway.ie

¹ Biomechanics Research Centre, Biomedical Engineering, College of Engineering and Informatics, National University of Ireland Galway, Galway, Ireland

² Boston Scientific, Ballybrit Business Park, Ballybrit, Galway, Ireland

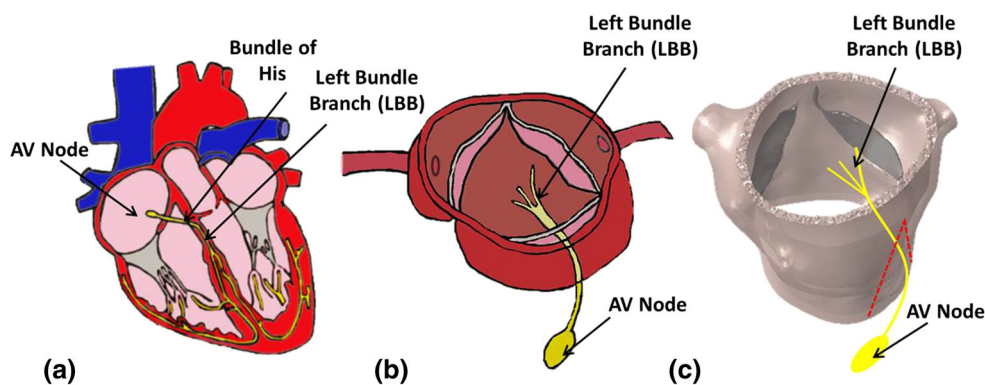


Fig. 1 **a** Schematic of the heart's conduction system, **b** schematic of the aortic valve and the region of the conduction system passing in close proximity to the aortic valve complex, **c** the patient-specific model of

aortic sinus with schematic representing the AV node and left bundle branch and the path where they pass in close proximity to the valve complex

ies) (Colombo and Latib 2012) and 25–85% (738 patients in 11 studies) for the self-expanding Medtronic CoreValve (Colombo and Latib 2012). The impact of LBBB in patients with valvular disease has not been widely investigated; however, it has been indicated that TAVI-induced LBBB is an independent indicator of mortality (Houthuizen et al. 2012).

In the aortic valve complex, under the commissures of the native valve lie the interleaflet triangles. The triangle between the right- and non-coronary sinuses contains the bundle of His, which is a part of the heart's conduction system and an extension of the atrioventricular (AV) node (Fig. 1) (Charitos and Sievers 2013; Misfeld and Sievers 2007). It has been proposed that elevated tissue stresses can trigger an inflammatory response, particularly in this region of tissue in close proximity to the heart's conduction system, and can lead to risk of conduction interference (Finotello et al. 2017; Hunter et al. 2012). Indeed, the increase in incidence of LBBB in the Medtronic CoreValve versus the Edwards SAPIEN has been attributed to the long skirt of the device which may, depending on the position of the valve, directly interfere with the conduction pathway (Khawaja et al. 2011). It has been confirmed that deeper (sub-annular) implantation depths lead to increased risk of conduction disorders (Fraccaro et al. 2011). However, the precise stresses induced by TAVs in the region of the interleaflet triangle where LBBB arises are unknown.

Finite element modelling of realistic TAVI patient geometries has been applied to investigate tissue–frame interactions and to provide an enhanced understanding of specific procedural complications. Specifically, patient-specific modelling has previously been used to predict the biomechanical interaction between the TAV and the stenotic aortic root (Wang et al. 2012) and has successfully predicted aortic root rupture (Wang et al. 2015). Furthermore, it has been used in investigating paravalvular leakage and coronary occlusion (Capelli et al. 2012; Wang et al. 2012), asymmetric expansion and leaflet stresses (Gunning et al. 2014b; Sun

et al. 2010) and poor hemodynamic performance (Sirois et al. 2011). Finite element methods can provide an insight into the biomechanical reactions during TAVI deployment that cannot be assessed in vivo. Such methods have also been applied to investigate the role of positioning for first-generation TAVs. Using a finite element approach, it was predicted that a higher implantation depth of the Edwards SAPIEN valve leads to a decrease in leaflet coaptation area, an increase in stress distribution on the leaflets and stress distribution on the aortic wall (Auricchio et al. 2014). In a recent study, a Medtronic CoreValve was computationally implanted at different implantation depths and angles in a patient-specific aortic root. The results predicted that deviations in implantation depth can result in variances in the frame-root contact area (41.3%), maximum von Mises stress (12.7%), paravalvular orifice area (63.4%) and differences in leaflet coaptation (40.2%). All these factors can impact the post-operative device performance and durability (Morganti et al. 2016). Next-generation repositionable valves, such as the Lotus valve, are currently under design and development. However, it remains that the relationship between the positioning of the mechanically expanded repositionable Lotus valve and stresses in the aortic root, in particular in the interleaflet triangle, has not been widely investigated.

The objective of this research is to apply a patient-specific finite element model to investigate the effects of TAV positioning on stress distribution in the aortic root and the valve frame eccentricity. A finite element study was carried out to simulate the deployment of a Lotus valve into a patient-specific aortic root at three different implantation depths. The frame eccentricity and stress in the aortic root were compared, and an analysis of levels of stress arising in the vicinity of the bundle of His, as a function of implantation depth, was conducted.

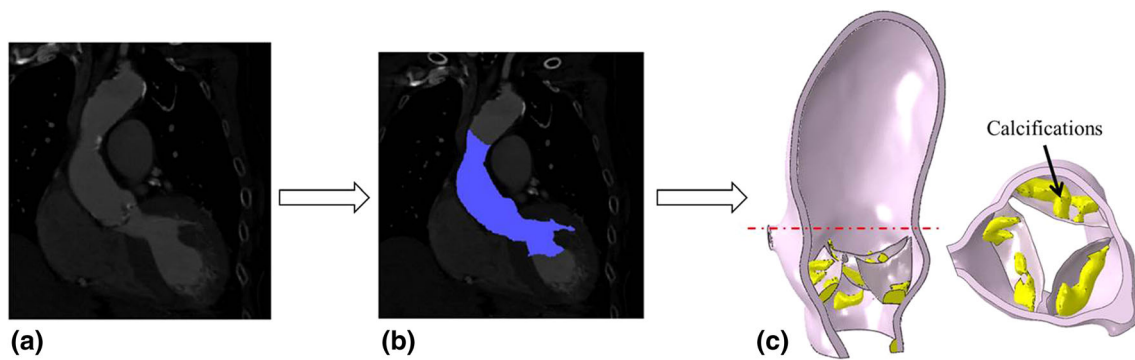


Fig. 2 Creation of the patient-specific aortic root geometry from **a** the MSCT scan of the aortic root, **b** segmentation of the aortic root using Mimics 14.1 to threshold the MSCT scans and **c** the final aortic root mesh including native leaflets and calcifications

2 Materials and methods

2.1 Aortic root model

In this study, a patient-specific aortic root geometry was reconstructed from multi-slice computed tomography (MSCT) images (Fig. 2). These images were obtained from an 81-year-old female with severe aortic stenosis and had a slice thickness of 0.750 mm, slice dimensions of 512×512 and pixel spacing of 0.5 mm. The MSCT scans were ECG gated to examine the 35% systolic phase. This was done to inform decisions regarding specific patient sizing criteria because it represents the point of maximum valve opening. Mimics 14.1 Imaging Software (Materialise, Leuven, Belgium) was used to threshold the leaflets, calcifications and aortic root (aortic sinus and ascending aorta) from the images.

Volume meshes of the aortic root and calcifications were generated using 3D continuum elements (4-noded tetrahedral elements with reduced integration (C3D4R)). The leaflets were meshed using shell elements with a thickness of 0.5 mm (Auricchio et al. 2014). The geometries were then imported into Abaqus/Explicit 6.13 (SIMULIA, Providence, RI). An assembly was then generated matching the corresponding nodal positions of the intersecting surfaces.

2.2 Lotus™ valve model

The Lotus valve frame geometry was created using SolidWorks (Fig. 3). This was then imported into Abaqus 6.13 as a wire part and meshed using 3-noded quadratic beam elements (B32). The overlap between the braids was modelled using spring connector elements.

2.3 Constitutive models

The Lotus valve frame was modelled using a superelastic material model. An Abaqus 6.13 inbuilt user subroutine

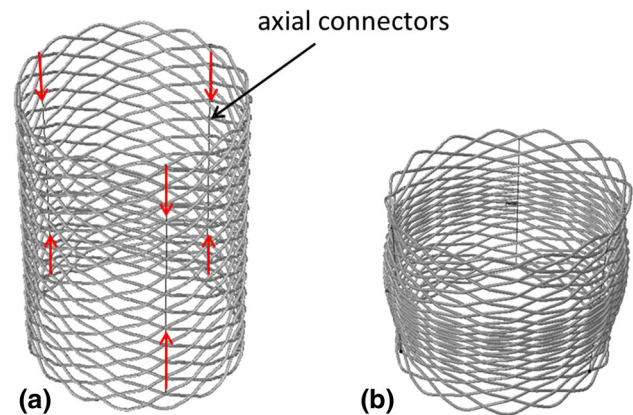


Fig. 3 Lotus™ valve frame geometry in **a** unlocked and **b** locked configuration

(VUMAT), based on the Auricchio and Taylor model, was used in assigning the superelastic properties (Auricchio and Taylor 1997; Auricchio et al. 1997). Using similar methods to those outlined by Tzamtzis et al. (2013), a numerical model was correlated to the experimental crush test of a nitinol Lotus valve frame.

The ascending aorta and the aortic sinus were modelled as isotropic hyperelastic materials. They were modelled using the first-order Ogden model (Ogden and Roxburgh 1999) fitted to uniaxial test data of human tissue (Martin et al. 2011; Wang et al. 2012) (Fig. 4; Table 1).

The calcifications were assumed to be isotropic and homogenous. The properties of atherosclerotic plaque were used due to the absence of aortic valvular calcification properties in the literature (Loree et al. 1994). A third-order Mooney–Rivlin hyperelastic material model was used, which is defined using strain energy function, U :

$$U = C_{10}(I_3 - 3) + C_{01}(I_2 - 3) + C_{20}(I_1 - 3)^2 + C_{11}(I_1 - 3)(I_2 - 3) + C_{30}(I_1 - 3)^3$$

Fig. 4 Experimental data versus model predictions for the stress–strain response of the human aortic sinus and ascending aorta

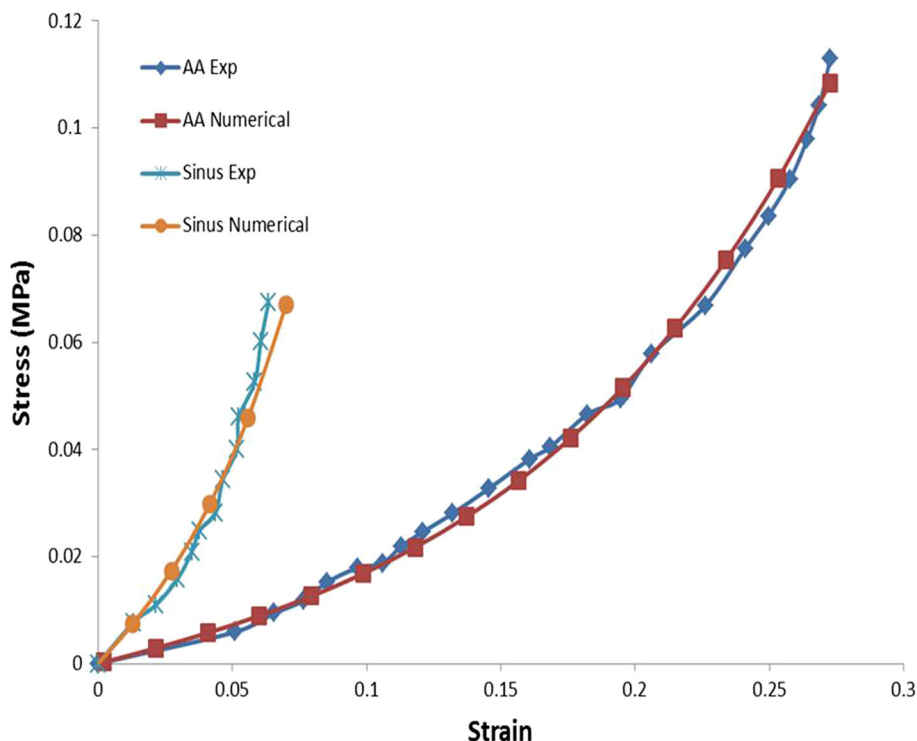


Table 1 Material parameters of human aortic sinus and ascending aorta

	μ 1	α 1	D1
Ascending aorta (AA)	0.0430	12.4814	0.4667
Sinus	0.1793	25.0000	0.1119

where I_1 and I_2 are first and second invariants of the Cauchy–Green tensor and C_{ij} are material constants. The material constants used were calibrated by Pericevic et al. (Pericevic et al. 2009) using data fitted to uniaxial data of atherosclerotic plaque by Loree et al. (Loree et al. 1994). The following material constants were used in the simulations presented: $C_{10} = 0.495$ MPa; $C_{01} = 0.51$ MPa; $C_{11} = 1.19$ MPa; $C_{20} = 3.64$ MPa and $C_{30} = 4.73$ MPa (Conway et al. 2012; Pericevic et al. 2009).

The aortic valve leaflets were modelled using a linear stress–strain relationship approximated from biaxial results of aortic valve leaflets tested in the circumferential direction with an elastic modulus of 1.6 MPa, a Poisson ratio of 0.495 and a density of 1140 kg/m³ (Gunning 2014; Wang et al. 2012).

2.4 Boundary conditions

The crimping and deployment of the frame were modelled in Abaqus 6.13 (SIMULIA, Providence, RI) using a cylindrical part [crimper (Fig. 5)], which was meshed using (SFM3D4R) 4-noded quadrilateral surface elements with reduced integra-

tion. A local cylindrical coordinate system was created to displace the crimper inward radially, see Fig. 5. The crimper was constrained axially and tangentially to prevent sliding. Zero friction contact was assigned to the interaction between the crimper and the frame. The crimper was assigned as the master surface, and the frame was assigned as the slave surface. The frame implantation depth was varied relative to the native aortic annulus, which was defined as a virtual ring connecting the three points of the leaflets at the base of each leaflet attachment (Kasel et al. 2013). The frame was first positioned annularly with an equal distribution of the frame positioned above and below the annulus (Case 1). During frame deployment, a coefficient of friction of 0.1 was used between the TAV frame (master) and the aortic root (slave) (Mummert et al. 2013). A third loading step was applied to the frame to simulate locking of the device, which is a feature of the repositionable mechanism in the Lotus valve (Figs. 3, 5). Three axial beam connector elements were placed to connect the locations of the buckles and the posts; an axial displacement was applied to join the buckles to the posts and lock the valve to a height of 19 mm (Fig. 6). This approach was repeated for the 5-mm supra-annular (Case 2) and sub-annular positions (Case 3). The top and bottom edges of the aortic root were constrained using non-displacement boundary conditions in the longitudinal and circumferential directions. The kinetic energy of the simulations was monitored to ensure that the ratio of kinetic energy to internal energy remained less than 5%.

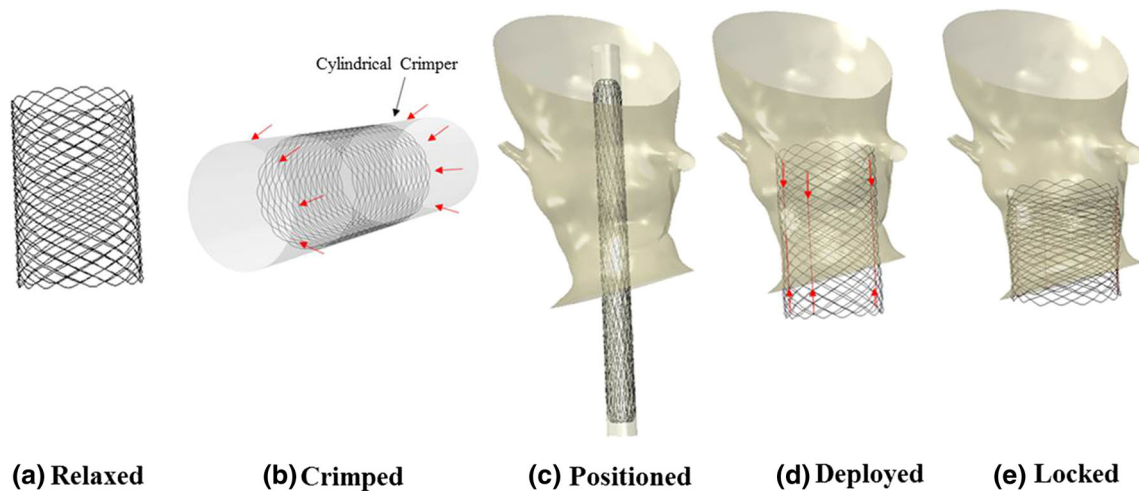


Fig. 5 Crimping and deployment method for the valve frame. **a** The frame in its relaxed position. **b** The crimping of the frame using a cylindrical crimper that is reduced inward radially and using contact crimps the frame to a diameter of 18FR. **c** The frame in its crimped configuration

positioned inside the aortic root. **d** The crimp is expanded allowing the self-expansion of the nitinol frame and deployment into the aortic root. **e** The connector elements are displaced inward to lock the frame to a height of 19 mm

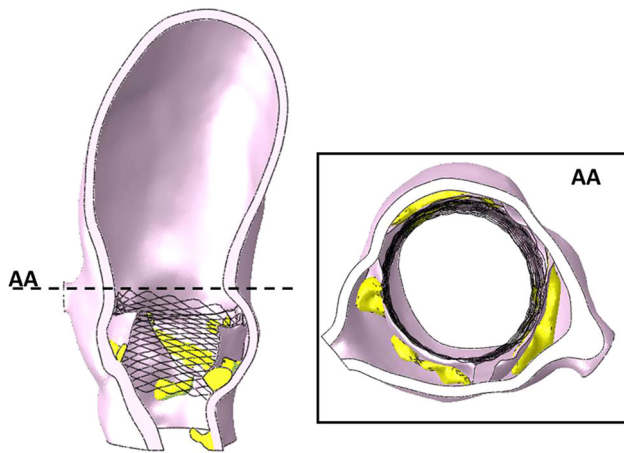


Fig. 6 Locked Lotus™ valve post-deployment in the calcified aortic root geometry

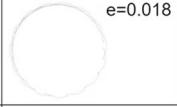

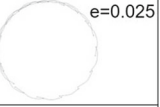
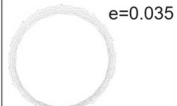
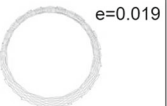

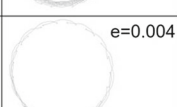
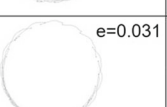
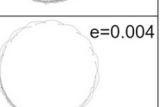
	5mm Sub	Annular	5mm Supra
Inflow	 e=0.018	 e=0.012	 e=0.025
Middle	 e=0.035	 e=0.019	 e=0.023
Outflow	 e=0.004	 e=0.031	 e=0.004

Fig. 7 Section views of the frame eccentricity throughout the frame at the inflow, mid-plane and outflow portions of the frame for the different deployment conditions where *e* denotes frame eccentricity

3 Results

3.1 Eccentricity

Eccentric valve geometries cause leaflet distortion, which can alter leaflet kinematics and fluid mechanics (Gunning et al. 2014a, b, 2015). The eccentricity of the valve frame was measured at the inflow, mid-plane and outflow segments of the Lotus valve frame using Eq. 1 (Gooley et al. 2015).

$$e = 1 - \left(\frac{D_{\min}}{D_{\max}} \right) \tag{1}$$

where D_{\max} and D_{\min} are the major and minor axes of the ellipse, respectively, and zero is the optimal eccentricity.

The D_{\max} and D_{\min} were measured by mapping an ellipse shape onto the stent cross section. Figure 7 demonstrates images of the cross sections from which the measurements were taken. Comparing the eccentricities at the inflow position, the location of the basal leaflet attachment, it was found that the annular position had the lowest eccentricity (0.012). The eccentricity increased to 0.018 at the 5-mm sub-annular position and 0.025 at 5-mm supra-annular (Fig. 7). The average frame eccentricity at each of the three positions (average of inflow, middle and outflow) was found to be 0.019 for the sub-annular position, 0.012 for the annular position and 0.017 for the supra-annular position. Upon examining the average eccentricity for the three positions, the average frame eccentricity was 0.005 at the outflow position versus 0.026 at the midpoint of the frame and 0.018 at the inflow position.

3.2 Aortic root peak stress and stress distribution

The peak von Mises stresses in the aortic sinus following initial frame deployment were examined at the three different deployment positions. Table 2 shows the peak stress and 99th percentile stresses (σ_{99}) in the aortic sinus and the average stress in the sinus (σ_{avg}) and the average stress in the interleaflet triangle (σ_{avg_int}). The peak stress in the aortic sinus was found to be the highest when the frame was positioned supra-annularly (1.141 MPa). The peak stress was lowest (0.892 MPa) when the frame was deployed 5 mm sub-annularly. A peak stress of 1.035 MPa was found when the frame was positioned at the 5-mm supra-annular position.

Figure 8 shows contour plots of the von Mises stress distribution throughout the aortic sinus. From the contour plots, we can see that the highest stress concentrations are located in the region where calcification is present. As the valve is implanted supra-annularly, the calcification on the right-coronary leaflet is further compressed against the wall of the aortic sinus leading to the maximum peak stress when the frame is implanted 5 mm supra-annularly. Figure 9 shows the contour plots of the von Mises stress distribution throughout the aortic sinus and in particular in the interleaflet triangle between the non-coronary and right-coronary sinus. It was found that as the valve is deployed at higher implantation depths, the amount of stress in the interleaflet triangle reduces. The percentage volume plots in Fig. 10 show the stress distribution throughout the interleaflet triangle for the three different positions following deployment of the Lotus valve frame. Comparing the volume of tissue above average stress (0.025–0.031 MPa), it was found that the percentage volume of tissue under higher stress increases when the frame is implanted at the 5-mm sub-annular versus 5-mm supra-annular and annular positions.

4 Discussion

In this study, finite element methods were applied to examine how positioning of a Lotus valve frame determined stress distribution in a patient-specific aortic root geometry, particularly focusing on the interleaflet triangle in which the bundle of His resides. Our results showed that TAV positioning had an influence on both the peak stresses in the aortic sinus and frame eccentricity. The results of this study also showed the

potential for finite element methods to predict levels of stress arising in the vicinity of the bundle of His, as a function of implantation depth. It was found that, for the specific patient anatomy studied, the 5-mm sub-annular position showed the lowest peak stress of the three implantation positions; however, this position led to the highest stress concentrations in the interleaflet triangle between the non-coronary and right-coronary sinus suggesting the highest potential for conductance interferences. In contrast, the 5-mm supra-annular position predicted decreased stress in the interleaflet triangle reducing the risk of conductance interference, while this position had the highest peak arterial stress. These results provide pre-operative information that can inform clinical decision-making regarding TAVI positioning and may lead to further insight into the underlying mechanobiological mechanisms that may cause conductance abnormalities.

There are limitations to this study. Firstly, the assumption was made that the aortic root is an isotropic hyperelastic material, although the aortic root is known to be anisotropic. However, the constitutive laws used were fitted to the circumferential direction, the stiffest directions of the aortic root, and it is known that the aortic root responds to deployment of the frame predominantly in the circumferential direction. Therefore, the use of an isotropic model was considered to be appropriate for correctly capturing the stress in this model (Gunning et al. 2014b; Zahedmanesh et al. 2010). Indeed, a recent study suggests that more complex models [i.e. Holzapfel–Gasser–Ogden (HGO)] do not necessarily lead to more accurate results as constitutive models cannot be adopted to represent material data from a specific patient (Finotello et al. 2017). Moreover, due to limited knowledge of patient-specific aortic pressure, aortic wall pre-stress was neglected. These assumptions may lead to an increase in predictions of the deformations in the aortic sinus (Hsu and Bazilevs 2011; Morganti et al. 2016). It must also be noted that the supra-annular position would not be a target implantation position in a clinical case using the Lotus valve, as it might result in an insufficient seal in the annulus and may lead to increased paravalvular leakage. However, due to the fact that this study did not model the paravalvular seal or examine paravalvular leakage, this position was used to examine an extreme case of mal-positioning. Furthermore, the model did not specifically include the buckles and posts of the repositionable mechanism of the Lotus valve frame. However, the buckles and posts are located on the inner portion of the

Table 2 Peak von Mises stress at different positions for the Lotus™ valve frame

(MPa)	Peak stress sinus	σ_{99} sinus	σ_{avg} sinus	σ_{avg_int} stress frame
5-mm supra-annular	1.141	0.131	0.024	0.025
Annular	1.035	0.148	0.027	0.030
5-mm sub-annular	0.892	0.126	0.027	0.031

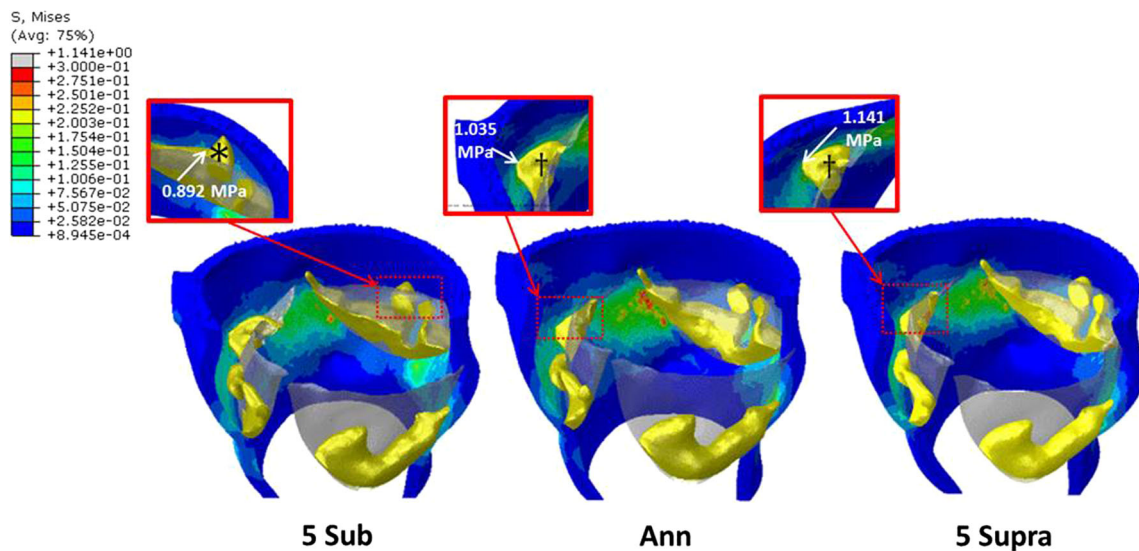


Fig. 8 Contour plots of the peak von Mises stress and corresponding calcification. In the 5-mm sub-annular position, a peak stress of 0.892 MPa was caused by compression of the calcium deposit (indicated by *) located on the non-coronary cusp. When the valve is implanted in the annular position, a higher peak stress was predicted (1.035 MPa) due

to another piece of calcium on the right-coronary cusp (indicated by †). However, when the valve was implanted at the 5-mm supra-annular position, the frame applied a greater force to the same calcium deposit (†) leading to the highest peak stress (1.141 MPa) at the 5-mm annular position

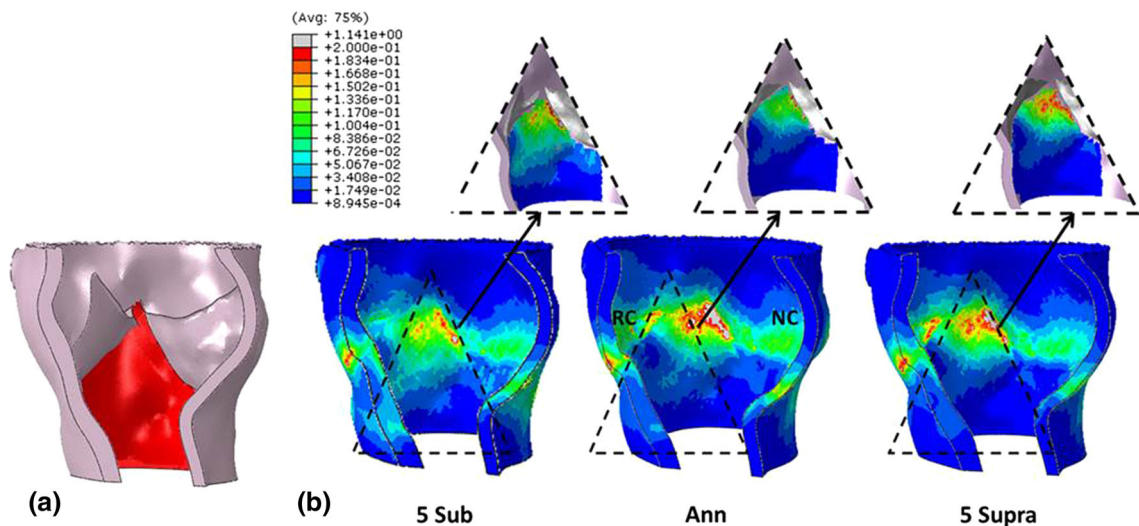


Fig. 9 a The area in red defined as the interleaflet triangle between the non-coronary (NC) and right-coronary (RC) sinus. **b** Contour plots of von Mises stress distribution throughout the aortic sinus and the inter-

leaflet triangle between the non-coronary (NC) and right-coronary (RC) sinus following deployment of the Lotus™ valve frame at the different implantation positions

frame and thus do not directly affect stress in the aortic tissue. Finally, in this study only one patient-specific anatomy was examined, and as such the specific results regarding the relationship between implantation depth and aortic tissue stress cannot be assumed to represent the entire population. However, this is the first detailed analysis to provide an understanding of the impact of TAV positioning for stress elevation in the vicinity of the bundle of His.

The results of this study show that positioning of the frame is important for frame eccentricity with the eccentric-

ity ranging between 0.004 and 0.035 based on variations in the position of the frame. Eccentricity is a metric commonly used to measure the level of frame distortion. Eccentricity should be taken into consideration in pre-operative planning, as eccentric frame geometries lead to leaflet distortion, altering leaflet kinematics and fluid mechanics (Gunning et al. 2014a, b, 2015). However, in this study the eccentricities shown by the Lotus valve frame are low and the device seems to retain its circular geometry even in an eccentric aortic root. In a study investigating the positioning strat-

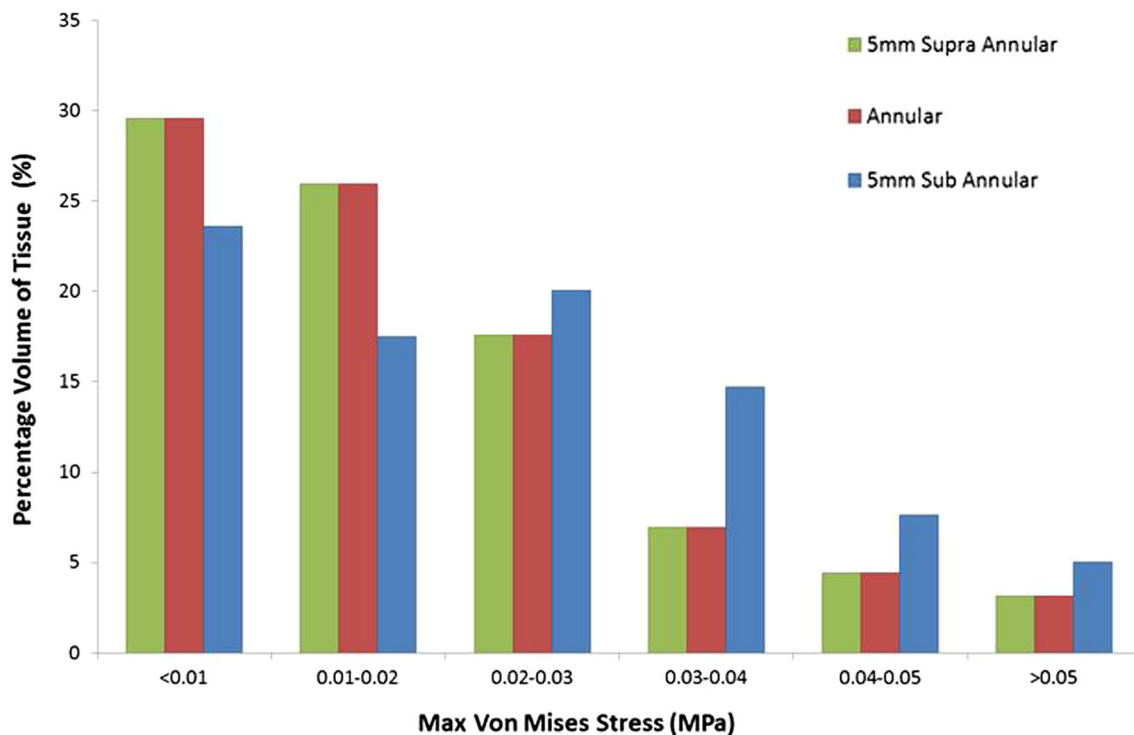


Fig. 10 Percentage of volume graph for the three different positions showing the stress distribution throughout the interleaflet triangle between the non-coronary and right-coronary sinus following deployment of the Lotus valve frame

egy of the CoreValve, it was found that the eccentricities ranged from 0.03 to 0.18 depending on implantation position (Morganti et al. 2016). The results of this study are in agreement with clinical results of the Lotus valve reporting average eccentricities of 0.06 ± 0.04 (Gooley et al. 2015), suggesting that the locking mechanism in the Lotus valve reduces frame eccentricity. Future investigation should be carried out into the potential of the locking mechanism in the Lotus valve to allow a self-expanding frame to keep a more rigid shape which may lead to a reduction in leaflet distortion while maintaining reduced volumes of paravalvular leakage.

A previous study found that when the Edward SAPIEN valve was positioned at higher and lower implantation depths the maximum von Mises stresses in the aortic root wall were found to be 0.98 MPa and 0.76 MPa at the lower and higher implantation depths, respectively (Auricchio et al. 2014). Another study examining the implantation depth of the CoreValve found that the average stresses (σ_{avg}) in the aortic root ranged from 0.034 MPa to 0.046 MPa at different implantation depths (Morganti et al. 2016). The current study reported higher peak stress (0.892–1.141 MPa) in the aortic sinus tissue compared to (Auricchio et al. 2014), but it must be noted that our model included native leaflets and calcification, and as such an increase in peak stress would be expected. The current study reported average stresses (0.024–0.027 MPa) in the same magnitude as (Morganti et al. 2016). It should be noted that the peak stresses predicted in

the aortic root for all three positions are well below the ultimate tensile stress of the aortic sinus, which has been found to range from 2.3 to 3.1 MPa (Wang et al. 2015).

Examining the peak stress in the aortic root, it appears as though the predominant cause of the peak stress is the result of calcium being pushed against the wall of the aortic sinus (Fig. 8). The peak stress in the 5-mm sub-annular position (0.892 MPa) was in the position of a calcium deposit (Fig. 8) located on the non-coronary leaflet. When the valve was implanted in the annular position, a higher peak stress was predicted (1.035 MPa) due to another piece of calcium on the right-coronary leaflet. However, when the valve was implanted at the 5-mm supra-annular position the frame applied a greater force to the same calcium deposit leading to the highest peak stress (1.141 MPa) at the 5-mm supra-annular position. These results would suggest that the peak stresses in the aortic sinus are dependent on the position on the valve relative to the location of calcium around the aortic root. It has previously been hypothesised that compression of calcification into the aortic root is the cause of aortic rupture in TAVI cases (Hayashida et al. 2013) and that calcium might be a useful predictor of aortic root rupture, and our results corroborate this hypothesis.

During clinical practice, the depth of the prosthesis has been shown to be an independent predictor of persistent LBBB, with lower positioning of the valve been shown to increase risk of conductance interference and the need for

permanent pacemaker implantation in both self-expanding and balloon-expandable valves (Baan et al. 2010; Urena et al. 2012). The results shown here illustrate that, while peak stress were lowest in the sub-annular positioning, there was no considerable difference in the average stress (σ_{avg}) in the aortic sinus with a σ_{avg} of 0.027 MPa in the annular and 5-mm sub-annular positions and a σ_{avg} of 0.024 MPa in the 5-mm supra-annular position (Table 2). For this reason, we decided to further investigate stress in areas that have greater potential for conductance interference, particularly under the commissures of the right- and non-coronary sinuses, the interleaflet triangle in close proximity to the bundle of His (Fig. 9). Interestingly, examining Fig. 9 we can see that the bands of higher stress move supra-annularly with higher implantation depth. Examining the average stress in the interleaflet triangle (σ_{avg_int}), they were found to be 0.031 MPa sub-annularly, 0.030 MPa annularly and 0.025 MPa supra-annularly. We further examined the stress in this area using percentage volume plots examining the volume of tissue under different bands of stress in this area (Fig. 10). It was predicted that when the valve is positioned supra- versus sub-annularly the percentage volume of tissue above the average stress considerably decreases in the interleaflet triangle. The results provide the first quantitative evidence in support of supra-annular positioning to reduce stress in the area where the conductance system is located. Thus, while peak stress is an indicator for aortic root rupture, it is not indicative of problems such as conductance interferences, which have been associated with damage to the surrounding tissue. Further, investigations of stress in patients with and without conductance interference may lead to a greater insight into the thresholds of stress that may lead to conductance interference.

5 Conclusion

In this study, we created a finite element model simulating the deployment of a Lotus valve frame into a calcified patient-specific aortic root geometry. This model was applied to investigate the effect of implantation depth on stress in the TAV and in the aortic root. Furthermore, we examined the potential of the Lotus valve locking mechanism in reducing the eccentricity of the valve frame. The results of this study predicted that the locking mechanism of the Lotus valve frame appears to work in reducing eccentricity maintaining circularity post-deployment. We predicted that while calcification patterns specific to this patient lead to the highest peak stress in the supra-annular position, this position led to the lowest stress in the interleaflet triangle in which the conductance system (bundle of His) resides, which provides the first quantitative evidence in support of the supra-annular position as the most appropriate Lotus valve implantation position for stress reduction in the vicinity of the conductance system.

These results show the potential for computational modelling techniques as a post-operative tool, providing clinicians with more informed procedural planning.

Acknowledgements The authors acknowledge funding from the Irish Researcher Council Enterprise Partnership Scheme Postgraduate Scholarship and the Irish Centre for High-End Computing (ICHEC).

Funding This study was funded by an Irish Research Council Enterprise Partnership Scheme Postgraduate Scholarship 2014 in collaboration with Boston Scientific (EPSPG/2014/120).

Compliance with ethical standards

Conflict of interest Orla M. McGee and Professor Laoise M. McNamara are collaborating with Boston Scientific under an Irish Research Council Enterprise Partnership Scheme Postgraduate Scholarship.

Ethical approval This article does not contain any studies with human participants or animals performed by any of the authors.

References

- Auricchio F, Taylor RL (1997) Shape-memory alloys: modelling and numerical simulations of the finite-strain superelastic behavior. *Comput Methods Appl Mech Eng* 143:175–194. [https://doi.org/10.1016/S0045-7825\(96\)01147-4](https://doi.org/10.1016/S0045-7825(96)01147-4)
- Auricchio F, Taylor RL, Lubliner J (1997) Shape-memory alloys: macromodelling and numerical simulations of the superelastic behavior. *Comput Methods Appl Mech Eng* 146:281–312. [https://doi.org/10.1016/S0045-7825\(96\)01232-7](https://doi.org/10.1016/S0045-7825(96)01232-7)
- Auricchio F, Conti M, Morganti S, Reali A (2014) Simulation of transcatheter aortic valve implantation: a patient-specific finite element approach. *Comput Methods Biomech Biomed Eng* 17:1347–1357. <https://doi.org/10.1080/10255842.2012.746676>
- Baan J Jr et al (2010) Factors associated with cardiac conduction disorders and permanent pacemaker implantation after percutaneous aortic valve implantation with the CoreValve prosthesis. *Am Heart J* 159:497–503. <https://doi.org/10.1016/j.ahj.2009.12.009>
- Block PC (2010) Leaks and the “great ship” TAVI. *Catheter Cardiovasc Interv* 75:873–874. <https://doi.org/10.1002/ccd.22581>
- Cao C, Ang SC, Vally MP, Ng M, Adams M, Wilson M (2012) Migration of the transcatheter valve into the left ventricle. *Ann Cardiothorac Surg* 1:243–244. <https://doi.org/10.3978/j.issn.2225-319X.2012.07.11>
- Capelli C et al (2012) Patient-specific simulations of transcatheter aortic valve stent implantation. *Med Biol Eng Compu* 50:183–192. <https://doi.org/10.1007/s11517-012-0864-1>
- Charitos EI, Sievers H-H (2013) Anatomy of the aortic root: implications for valve-sparing surgery. *Ann Cardiothorac Surg* 2:53–56
- Colombo A, Latib A (2012) Left bundle branch block after transcatheter aortic valve implantation inconsequential or a clinically important endpoint? *J Am Coll Cardiol* 60:1753–1755. <https://doi.org/10.1016/j.jacc.2012.07.034>
- Conway C, Sharif F, McGarry JP, McHugh PE (2012) A computational test-bed to assess coronary stent implantation mechanics using a population-specific approach. *Cardiovasc Eng Technol* 3:374–387. <https://doi.org/10.1007/s13239-012-0104-8>
- Finotello A, Morganti S, Auricchio F (2017) Finite element analysis of TAVI: impact of native aortic root computational modeling strate-

- gies on simulation outcomes. *Med Eng Phys* 47:2–12. <https://doi.org/10.1016/j.medengphy.2017.06.045>
- Fraccaro C et al (2011) Incidence, predictors, and outcome of conduction disorders after transcatheter self-expandable aortic valve implantation. *Am J Cardiol* 107:747–754. <https://doi.org/10.1016/j.amjcard.2010.10.054>
- Généreux P et al (2013) Paravalvular leak after transcatheter aortic valve replacement the new Achilles' heel? A comprehensive review of the literature. *J Am Coll Cardiol* 61:1125–1136. <https://doi.org/10.1016/j.jacc.2012.08.1039>
- Gooley RP, Cameron JD, Meredith IT (2015) Assessment of the geometric interaction between the lotus transcatheter aortic valve prosthesis and the native ventricular aortic interface by 320-multidetector computed tomography. *JACC Cardiovasc Interv* 8:740–749. <https://doi.org/10.1016/j.jcin.2015.03.002>
- Gunning P (2014) Experimental and computational investigation of the impact of distorted stent expansion on the performance of transcatheter aortic valve replacements. NUI Galway
- Gunning PS, Saikrishnan N, McNamara LM, Yoganathan AP (2014a) An in vitro evaluation of the impact of eccentric deployment on transcatheter aortic valve hemodynamics. *Ann Biomed Eng* 42:1195–1206. <https://doi.org/10.1007/s10439-014-1008-6>
- Gunning PS, Vaughan TJ, McNamara LM (2014b) Simulation of self expanding transcatheter aortic valve in a realistic aortic root: implications of deployment geometry on leaflet deformation. *Ann Biomed Eng* 42:1989–2001. <https://doi.org/10.1007/s10439-014-1051-3>
- Gunning PS, Saikrishnan N, Yoganathan AP, McNamara LM (2015) Total ellipse of the heart valve: the impact of eccentric stent distortion on the regional dynamic deformation of pericardial tissue leaflets of a transcatheter aortic valve replacement. *J R Soc Interface* 12:20150737. <https://doi.org/10.1098/rsif.2015.0737>
- Hayashida K et al (2013) Potential mechanism of annulus rupture during transcatheter aortic valve implantation. *Catheter Cardiovasc Interv* 82:E742–746. <https://doi.org/10.1002/ccd.24524>
- Houthuizen P et al (2012) Left bundle-branch block induced by transcatheter aortic valve implantation increases risk of death. *Circulation* 126:720–728. <https://doi.org/10.1161/circulationaha.112.101055>
- Hsu M-C, Bazilevs Y (2011) Blood vessel tissue prestress modeling for vascular fluid–structure interaction simulation. *Finite Elem Anal Des* 47:593–599. <https://doi.org/10.1016/j.finel.2010.12.015>
- Hunter RJ, Liu Y, Lu Y, Wang W, Schilling RJ (2012) Left atrial wall stress distribution and its relationship to electrophysiologic remodeling in persistent atrial fibrillation. *Circulation Arrhythm Electrophysiol* 5:351
- Jung B et al (2003) A prospective survey of patients with valvular heart disease in Europe: the Euro heart survey on valvular heart disease. *Eur Heart J* 24:1231–1243
- Kasel AM, Cassese S, Bleiziffer S, Amaki M, Hahn RT, Kastrati A, Sengupta PP (2013) Standardized imaging for aortic annular sizing implications for transcatheter valve selection. *JACC Cardiovasc Imaging* 6:249–262. <https://doi.org/10.1016/j.jcmg.2012.12.005>
- Khawaja MZ et al (2011) Permanent pacemaker insertion after core valve transcatheter aortic valve implantation. *Circulation* 123:951
- Loree HM, Grodzinsky AJ, Park SY, Gibson LJ, Lee RT (1994) Static circumferential tangential modulus of human atherosclerotic tissue. *J Biomech* 27:195–204
- Martin C, Pham T, Sun W (2011) Significant differences in the material properties between aged human and porcine aortic tissues. *Eur J Cardiothorac Surg* 40:28–34. <https://doi.org/10.1016/j.ejcts.2010.08.056>
- Masson J-B et al (2009) Transcatheter aortic valve implantation review of the nature, management, and avoidance of procedural complications. *JACC Cardiovasc Interv* 2:811–820. <https://doi.org/10.1016/j.jcin.2009.07.005>
- Misfeld M, Sievers H-H (2007) Heart valve macro- and microstructure. *Philos Trans R Soc B Biol Sci* 362:1421–1436. <https://doi.org/10.1098/rstb.2007.2125>
- Morganti S, Brambilla N, Petronio AS, Reali A, Bedogni F, Auricchio F (2016) Prediction of patient-specific post-operative outcomes of TAVI procedure: the impact of the positioning strategy on valve performance. *J Biomech*. <https://doi.org/10.1016/j.jbiomech.2015.10.048>
- Mummert J, Sirois E, Sun W (2013) Quantification of biomechanical interaction of transcatheter aortic valve stent deployed in porcine and ovine hearts. *Ann Biomed Eng* 41:577–586
- Ogden RW, Roxburgh DG (1999) A pseudo-elastic model for the Mullins effect in filled rubber. *Proc R Soc Lond Ser A Math Phys Eng Sci* 455:2861
- Pericevic I, Lally C, Toner D, Kelly DJ (2009) The influence of plaque composition on underlying arterial wall stress during stent expansion: the case for lesion-specific stents. *Med Eng Phys* 31:428–433. <https://doi.org/10.1016/j.medengphy.2008.11.005>
- Piazza N, de Jaegere P, Schultz C, Becker AE, Serruys PW, Anderson RH (2008) Anatomy of the aortic valvar complex and its implications for transcatheter implantation of the aortic valve. *Circ Cardiovasc Interv* 1:74–81. <https://doi.org/10.1161/circinterventions.108.780858>
- Sirois E, Wang Q, Sun W (2011) Fluid simulation of a transcatheter aortic valve deployment into a patient-specific aortic root. *Cardiovasc Eng Technol* 2:186–195. <https://doi.org/10.1007/s13239-011-0037-7>
- Sun W, Li K, Sirois E (2010) Simulated elliptical bioprosthetic valve deformation: implications for asymmetric transcatheter valve deployment. *J Biomech* 43:3085–3090. <https://doi.org/10.1016/j.jbiomech.2010.08.010>
- Tzamtzis N, Viquerat J, Yap J, Mullen MJ, Burriesci G (2013) Numerical analysis of the radial force produced by the Medtronic-CoreValve and Edwards-SAPIEN after transcatheter aortic valve implantation (TAVI). *Med Eng Phys* 35:125–130. <https://doi.org/10.1016/j.medengphy.2012.04.009>
- Urena M et al (2012) Predictive factors and long-term clinical consequences of persistent left bundle branch block following transcatheter aortic valve implantation with a balloon-expandable valve. *J Am Coll Cardiol* 60:1743–1752. <https://doi.org/10.1016/j.jacc.2012.07.035>
- Walther T, Blumenstein J, van Linden A, Kempfert J (2012) Contemporary management of aortic stenosis: surgical aortic valve replacement remains the gold standard. *Heart* 98(Suppl 4):iv23–29. <https://doi.org/10.1136/heartjnl-2012-302399>
- Wang Q, Sirois E, Sun W (2012) Patient-specific modeling of biomechanical interaction in transcatheter aortic valve deployment. *J Biomech* 45:1965–1971. <https://doi.org/10.1016/j.jbiomech.2012.05.008>
- Wang Q, Kodali S, Primiano C, Sun W (2015) Simulations of transcatheter aortic valve implantation: implications for aortic root rupture. *Biomech Model Mechanobiol* 14:29–38. <https://doi.org/10.1007/s10237-014-0583-7>
- Zahedmanesh H, John Kelly D, Lally C (2010) Simulation of a balloon expandable stent in a realistic coronary artery—determination of the optimum modelling strategy. *J Biomech* 43:2126–2132. <https://doi.org/10.1016/j.jbiomech.2010.03.050>

Publisher's Note Springer Nature remains neutral with regard to jurisdictional claims in published maps and institutional affiliations.